CELEBRATING 5 YEARS

ACS Photonics

FEBRUARY 2018
VOLUME 5
NUMBER 2
pubs.acs.org/acsphotonics

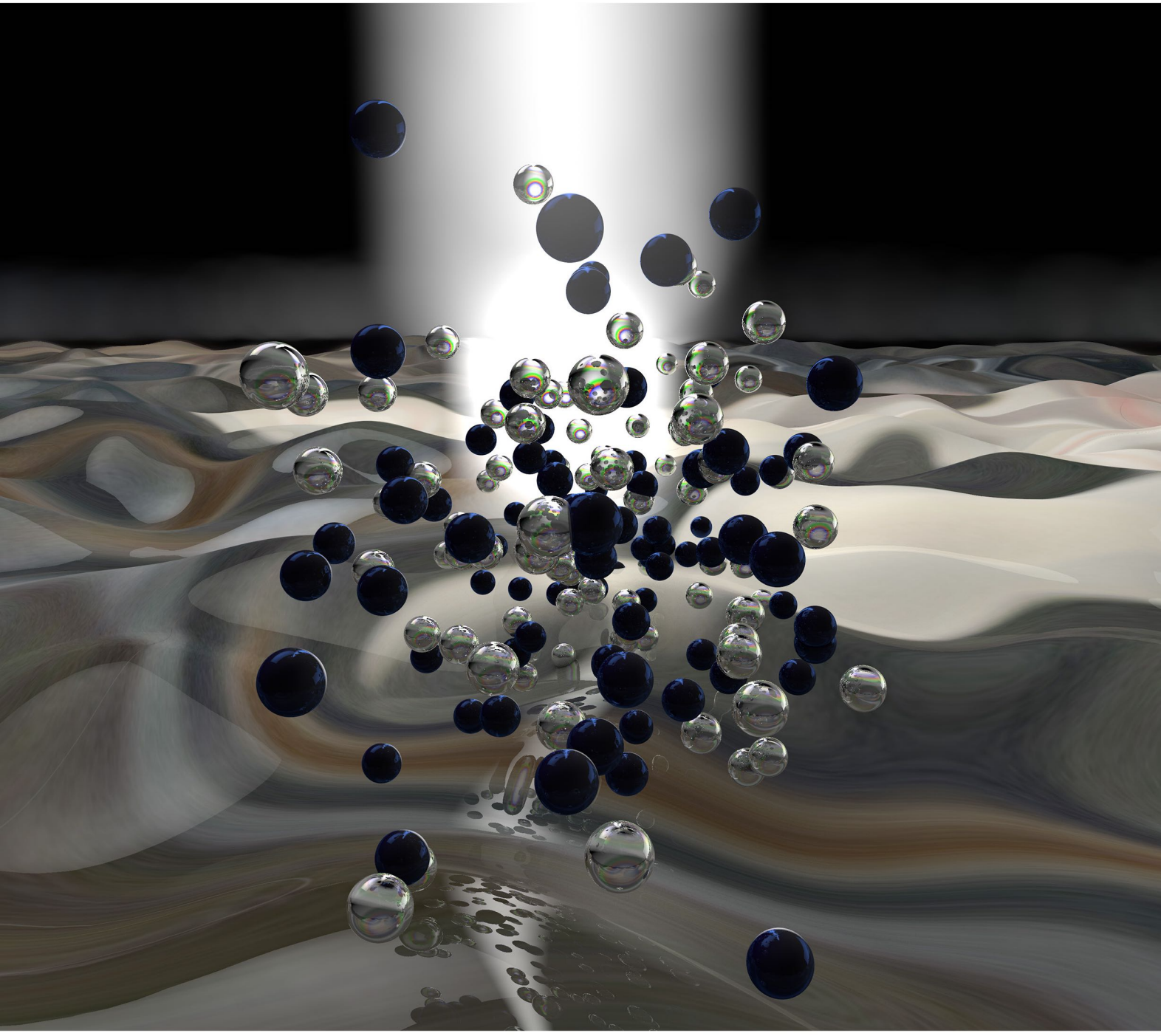

ACS Publications
Most Trusted. Most Cited. Most Read.

www.acs.org

ACS Photonics

Letter

pubs.acs.org/journal/apchd5

Near-IR Imaging Based on Hot Carrier Generation in Nanometer-Scale Optical Coatings

Lisa J. Krayer,[†,‡] Elizabeth M. Tennyson,[‡,§] Marina S. Leite,[‡,§] and Jeremy N. Munday*[,†,‡]

[†]Department of Electrical and Computer Engineering, [‡]Institute for Research in Electronics and Applied Physics, and [§]Department of Materials Science and Engineering, University of Maryland College Park, Maryland 20742, United States

Supporting Information

ABSTRACT: Silicon is the most widely used material for visible photodetection, with extensive applications in both consumer and industrial products. Further, its excellent optoelectronic properties and natural abundance have made it nearly ideal for microelectronic devices and solar cells. However, its lack of absorption in the infrared precludes its use in infrared detectors and imaging sensors, severely constraining its implementation in telecommunications. Here we show that this limitation can be overcome by exploiting resonant absorption in ultrathin metal films (<20 nm). Through appropriate optical design, a zeroth-order Fabry−Perot resonance is achieved, enabling ∼80% light absorption below the bandgap of the semiconductor. Absorption within the metal film results in excitation and injection of hot carriers through a Schottky junction into the Si. We experimentally demonstrate this phenomenon with four ultrathin planar metal films (Pt, Fe, Cr, and Ti), chosen to satisfy the resonant condition over a wide range of wavelengths (1200−1600 nm), and realize a near-infrared imaging detector. Our approach paves the way to implement a scalable, lithography free, and low-cost route to obtain silicon-based optoelectronics beyond the material bandgap.

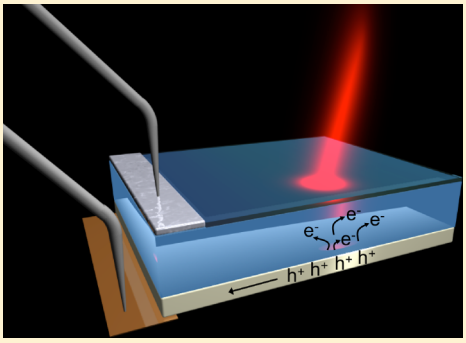

KEYWORDS: *photodetection, ultrathin films, hot electrons, Schottky detector, Fabry−Perot resonance, metal absorption*

Silicon (Si) has emerged as an important material for telecommunications, enabling hybrid optical and electrical components to be combined onto a single integrated chip.[1−3] It is a mature, low-cost technology that is dominant throughout the microelectronics industry. However, the bandgap of Si (E_g = 1.1 eV; λ_g = 1100 nm) severely constrains its use for generation and detection of light throughout the telecommunications band (1260−1625 nm). To circumvent this limitation, a second semiconducting material is often introduced, such as Ge to produce telecom lasers[4] and photodetectors,[5,6] III−V materials,[7] or GeSn alloys;[8,9] nevertheless, Si-only approaches are desirable because they can easily be incorporated with traditional fabrication methods. Options for Si-only sub-bandgap photodetection include increased absorption from intrinsic defect states within the Si bandgap,[10] induced defect states by ion implantation,[11] or photon absorption and internal electron emission from a metal film (typically metal silicides such as PtSi or pure metals such as Au or Cu) across a Schottky barrier.[12−15] However, one of the key drawbacks of internal electron emission is that it requires significant absorption within a thin metal film, which is usually highly reflective in the near-infrared (NIR) spectrum.[15,16] For example, metal silicides generally have little absorption and require low temperature operation because of high dark current due to small barrier heights. Nanostructured films and antennas can be used to increase the absorption but suffer from significant wavelength, polarization, and angle of incidence dependence.

Recently, it has been shown that ultrathin (∼10 nm) dielectric and semiconducting films can become nearly perfect absorbers based on nontrivial phase accumulation in lossy materials.[17−21] This phenomenon occurs by exciting Fabry−Perot (FP) resonances in cavities 10−100× smaller than the incident wavelength of light. Such films have been used to construct ultrathin color filters,[19,20] enhance photochemical water splitting efficiency,[22] and create near-unity perfect absorbers.[23,24] Despite these successes based on dielectric and semiconducting materials, expanding this concept to ultrathin metal films could enable near perfect NIR photon absorption for Schottky barrier photodetectors and allow for seamless integration to CMOS telecommunication applications.

Here, we demonstrate a Si-based photodetector that operates in the NIR, beyond the semiconductor bandgap, by exploiting a zeroth-order FP resonance in ultrathin metal films. The devices are composed of a Si/metal layer stack, where the lithography-free, ultrathin metallic layer generates photocurrent at room temperature in the NIR due to hot carrier (electron) generation. The devices absorb nearly 80% of the incident radiation beyond the Si bandgap and are broadband. We identify four metals that satisfy this resonance condition in the telecom band: Pt, Fe, Ti, and Cr. As a proof-of-concept, we fabricate and test Si/Pt photodetectors that outperform commercial Si devices in the NIR (>1.2 μm) and demonstrate

Received: September 7, 2017
Published: November 7, 2017

DOI: 10.1021/acsphotonics.7b01021
ACS Photonics 2018, 5, 306−311

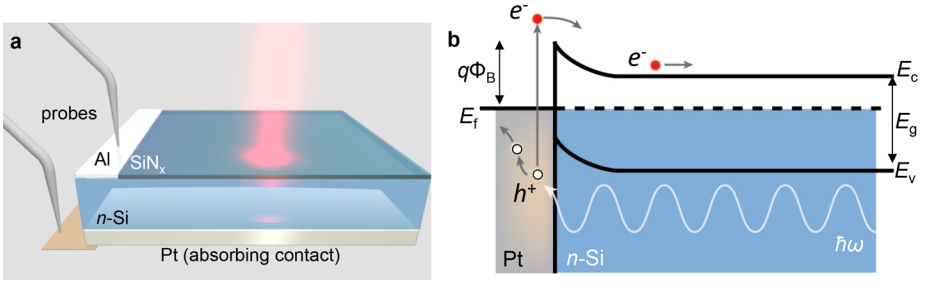

Figure 1. Hot carriers for Si photodetection beyond the material's bandgap. (a) Illustration of device structure, out of scale for clarity. From top to bottom: Al top Ohmic contact (left side only), antireflection coating (SiN_x), *n*-type Si layer, ultrathin Pt absorbing contact layer. Sub-bandgap light passes through the device to be absorbed in the thin back contact. Electrical connections are made to the top and bottom contacts. (b) Energy band diagram showing the hot carrier absorption concept: light with energy below the Si bandgap ($\hbar\omega < E_g$) is absorbed by the back metal contact (Pt), which generates hot electrons (e^-) that are injected into the semiconductor when their energy is greater than the barrier height $q\Phi_B$.

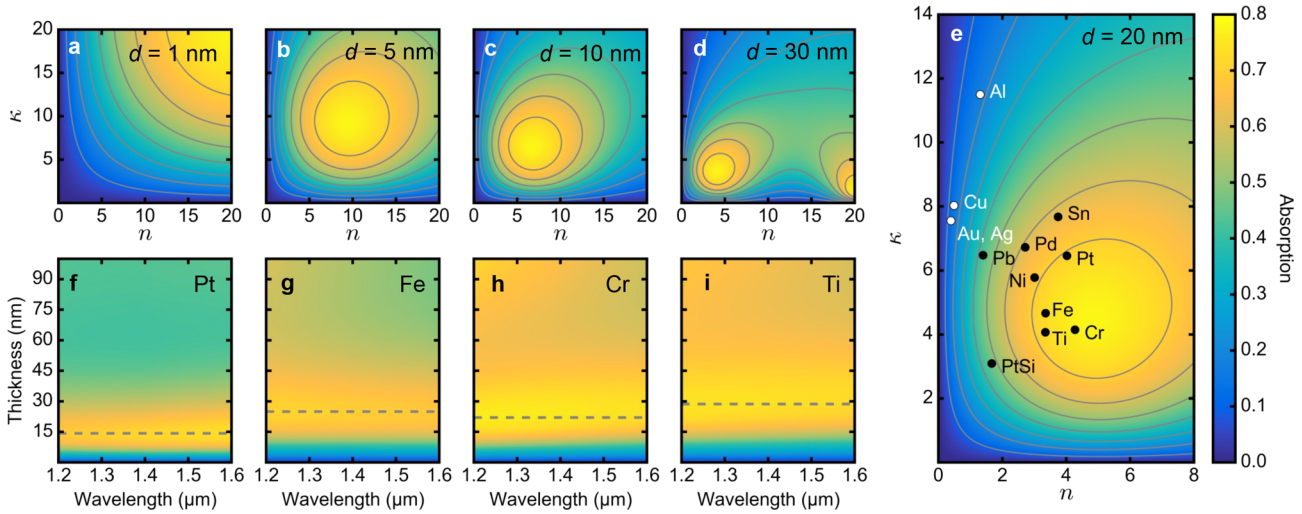

Figure 2. Light absorption in metallic ultrathin films. (a–d) Absorption contour plots as a function of $n = n_m + i\kappa_m$ for thin metal films with variable thicknesses (d = 1–30 nm) on the backside of bulk Si. Illumination (λ = 1.2 μm) is from free space through the SiN_x/Si layers. (e) Absorption contour plot for metal thin films with thickness d = 20 nm. Black and white dots denote refractive indices for common metals at λ = 1.2 μm, showing high absorption of selected metals. (f–i) Light absorption as a function of film thickness for Pt, Fe, Cr, and Ti, respectively. Greater than 50% absorption is achieved for films as thin as 10 nm. The dashed gray lines indicate the film thickness corresponding to maximum absorption, >74% in all cases.

their imaging capability. We foresee the development of low-cost, Si IR and NIR detectors for next-generation Si photonics based on our findings.

RESULTS AND DISCUSSION

Our device geometry, presented in Figure 1a, consists of an *n*-type Si substrate (368 μm thickness) and an ultrathin film metal (16 nm thick Pt) absorbing layer. In addition to providing optical absorption and hot carrier generation, the metal film acts as a Schottky contact for carrier injection. Al is used for the top Ohmic contact, and a SiN_x coating is added to the top of the Si layer to reduce reflection of the incident light. Figure 1b shows the device band diagram, where NIR photons with energy $\hbar\omega$ are resonantly absorbed within the metal before exciting hot carriers. These hot carriers are then directly injected into Si, if their excitation energy is greater than the barrier height ($q\Phi_B$).

We analytically determine the absorption of ultrathin metal films in contact with Si using Fresnel equations for a single stack of Si/metal/air for a variety of metals and layer thicknesses (d) at a wavelength of 1.2 μm (see Supporting Information, eqs 1–6, for calculation details). While the Fresnel equations are used for all quantitative analyses, additional insight can be gained by considering the following special case: (i) the surrounding layers are optically thick and nonabsorbing, (ii) the real (n) and imaginary (κ) parts of the metal's refractive index are large and approximately equal to each other (i.e., $n \approx \kappa \gg 0$), (iii) the refractive index of the top layer (n_{top}, here corresponding to Si) is greater than or equal to that of the bottom layer (n_{bot}, which corresponds to air in our case), and (iv) the optical path length in the metal film is significantly shorter than the wavelength of incident light (i.e., $d \ll \lambda_0/2\pi$, where λ_0 is the wavelength in air). Under these criteria, the maximum possible absorption in a metal film is determined by the optical properties of the surrounding layers:[17]

$$A_{max} \approx \frac{n_{top}}{n_{top} + n_{bot}} \quad (1)$$

When the top layer is Si and the bottom layer is air, it is possible to obtain significant light absorption (77.8%) in a metallic film 2 orders of magnitude thinner than the excitation wavelength.

The specific real and imaginary parts of the refractive indices that satisfy the requirements for maximum absorption shift to

DOI: 10.1021/acsphotonics.7b01021
ACS Photonics 2018, 5, 306–311

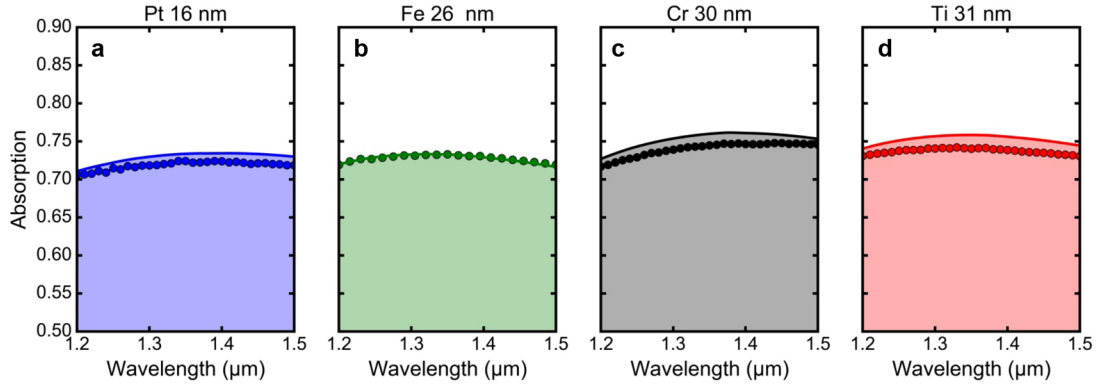

Figure 3. High optical absorption in metals due to a Fabry–Perot resonance. Measured (circles) and calculated (lines) absorption for (a) 16 nm of Pt, (b) 26 nm of Fe, (c) 30 nm of Cr, and (d) 31 nm of Ti in a Si/metal stack. Film thicknesses were chosen for maximum absorption.

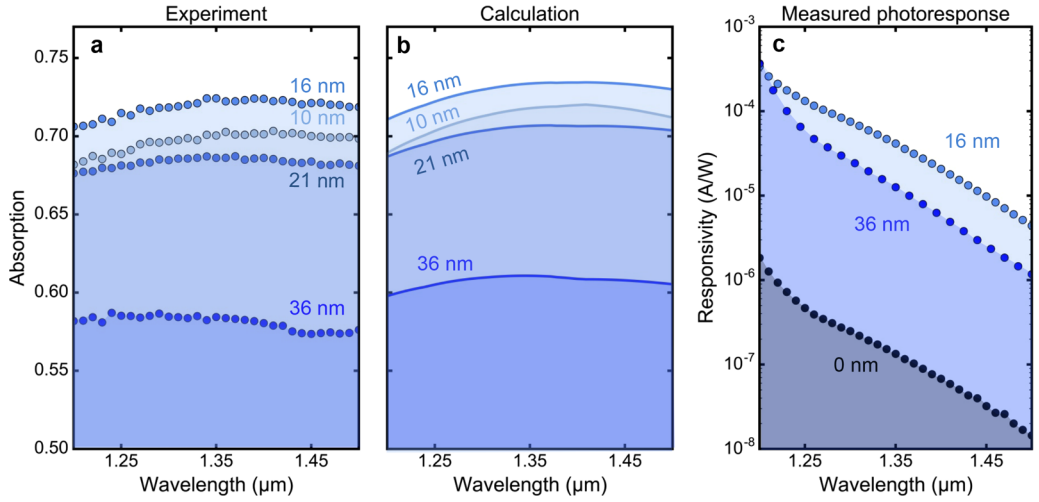

Figure 4. Ultrathin Pt layer leads to Si photodetection in the NIR. (a) Measured and (b) calculated absorption for 10, 16, 21, and 36 nm of Pt. Maximum absorption occurs for a Pt thickness of 16 nm. (c) Device photoresponse using 0, 16, and 36 nm of Pt. As expected, the 16 nm thick layer yields the highest photoresponse.

larger values along the $n = \kappa$ line as the film thickness decreases (see Figure 2). Note that 77.8% absorption can be achieved even in a film thickness of 1 nm, see Figure 2a. For this thickness, the optical indices of the material needs to satisfy $n \sim \kappa \sim 20$, for which there are no common metals. However, for larger thicknesses, still in the nanoscale regime, many common materials can meet the resonance condition. For example, at $d =$ 20 nm, platinum (Pt), iron (Fe), chromium (Cr), and titanium (Ti) lie near the absorption peak (Figure 2e). Analytical calculations for these materials show broadband absorption >70% for films as thin as 10 nm over a range of wavelengths throughout the NIR, see Figure 2f–i. The refractive indices for these calculations are taken from refs 25 and 26. The FP resonance is possible for these metals as long as $d \ll \lambda_0/2\pi$. Therefore, high absorption is maintained across a broadband of wavelengths because the metal film thicknesses are ~100× smaller than the incident light. Note that Pt maintains the highest absorption for the thinnest film.

Experimental Demonstration of High Absorption and Photocurrent in Ultrathin Metal Films. We measure the absorption in the four thin metal films with optimized thicknesses, as determined by the calculations in Figure 2f –i. Each sample is fabricated with an antireflection coating of 170 ± 5 nm of SiN_x on the top surface of a double sided polished Si wafer to reduce the incident light reflection from the Si, resulting in a minimum at a wavelength of 1.35 μm (see Methods and Supporting Information). The metal is deposited on the Si surface opposite of the SiN_x coating, forming a back Schottky contact, as depicted in Figure 1. Figure 3a–d presents the comparison of the experimental and analytical absorption in all four metals after including the loss due to reflection from the SiN_x. Each sample is illuminated from the SiN_x side. Cr has the highest absorption with an average value of 73.7%; however, the thickness required is double that of Pt, which has an average absorption of 71.5% in a thickness of merely 16 nm. As expected, if the sample orientation is reversed so that the metal is illuminated from the air rather than Si, the maximum absorption is reduced to 22%, in agreement with eq 1 for $n_{top} \sim 1$ (air) and $n_{bot} \sim 3.5$ (Si), see Supporting Information, Figures 1 and 3.

Pt is the most promising material for a hot carrier photodetector from the four options we investigated. The electron mean free paths of Pt and Fe are reported to be ~10 nm[27] and 2–8 nm,[27,28] respectively, and are comparable to the thickness of the ultrathin absorbers, whereas the electron mean free paths for Cr and Ti are expected to be <1 nm.[29] However, the expected barrier height for Fe in contact with n-Si is 0.45 eV, significantly lower than Pt, which leads to a large increase in dark current, thus reducing the photoresponse of the device at room temperature.[16] Because Pt achieves maximum absorption

DOI: 10.1021/acsphotonics.7b01021
ACS Photonics 2018, 5, 306–311

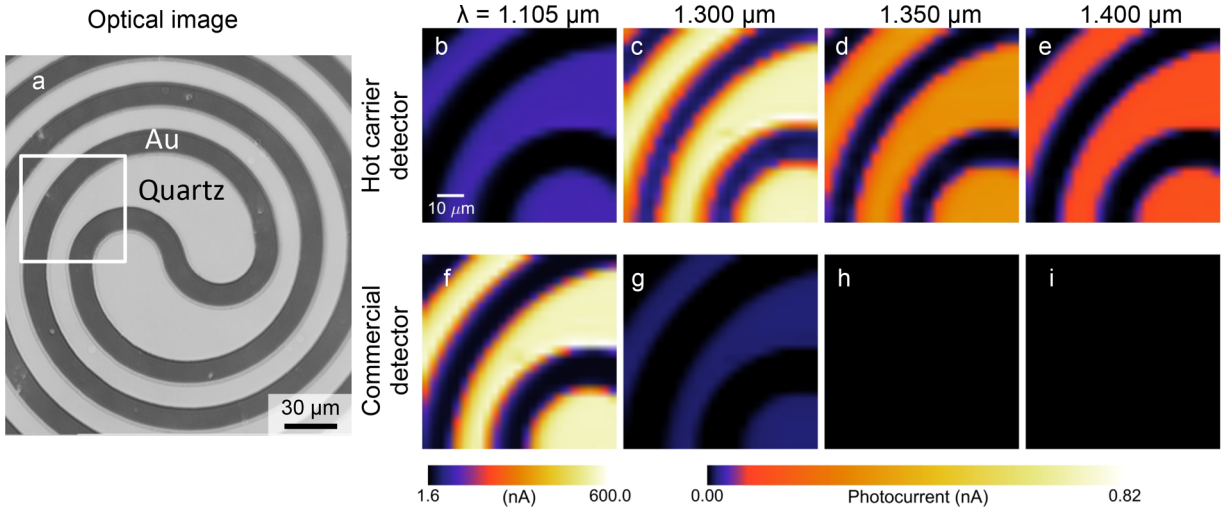

Figure 5. NIR imaging with the ultrathin film hot carrier photodetector. (a) Optical image of Au/Quartz structure, acquired using a 20× objective lens (NA = 0.4). The boxed region indicates the area imaged in (b−i). Images obtained by (b−e) the hot carrier photodetector consisting of 16 nm of Pt and (f−i) a commercial Si device. Beyond the Si bandgap, the hot carrier device outperforms the conventional Si photodetector.

for thinner layers, the probability for internal photoemission is potentially larger due to the increased likelihood of hot carrier reflection from the back surface.[30] Pt also has a larger Schottky barrier height to *n*-Si, which reduces the overall dark current, enabling room temperature detection.[16] In Figure 4a,b, we show measured and calculated absorption for various thicknesses of Pt to verify the optimal layer thickness for maximum absorption. A thickness of 16 nm results in a maximum, and changing the thickness by 5 nm reduces the absorption by only ∼2−5%, in excellent agreement with theory.

To efficiently generate hot electron photocurrent, the absorbed radiation should excite electrons to energy levels above the Schottky barrier for injection into the Si. The Schottky barrier height, $q\Phi_B$, for each Pt device varied between 0.69 and 0.72 eV, as determined from the dark *IV* measurements (see Supporting Information). To demonstrate the effect of the higher absorption on photoresponse, Figure 4c shows the measured photoresponse for devices with Pt thicknesses of 0, 16, and 36 nm. The 16 nm device has 2−3× larger photocurrent compared to the 36 nm one because of its higher absorption and greater probability of internal photoemission. The hot carrier devices are further compared with the photoresponse of bare Si, where the 10^{-6}−10^{-8} A/W photoresponse is likely due to trap states or two photon absorption; therefore, the hot carrier effect in Pt produces a 100× increase in photocurrent compared to the bare Si device. We also note that while the overall shape of the responsivity curve is similar for both the bare-Si device and the Pt devices, they result from different effects. The decrease in responsivity as a function of wavelength for the bare-Si device results from the continued decrease in the residual absorption beyond the bandgap. For the Pt devices, the absorption is nearly constant (Figure 4a,b); however, the internal quantum efficiency decreases as lower energy carriers are less likely to traverse the barrier.[31]

Near-Infrared Photodetector. We realize a NIR imaging photodetector based on the Pt hot carrier concept discussed in the previous paragraphs, which outperforms commercial Si devices. Figure 5a shows a backside-illuminated optical image of the "object" used to test our Si-based Pt photodetector, formed by an optically thick layer of Au in a spiral shape on top of a quartz substrate. The quartz is transparent for all incident wavelengths while the Au is opaque. Thus, it is expected that the regions coated by Au will appear dark to the photodetector, while the quartz appears bright. We compare the performance of our hot carrier device (Figure 5b−e) with a standard commercial Si detector (Figure 5f-i) for illumination near and below the bandgap of Si. Here, we use identical experimental conditions and place the detectors after an objective lens used to collect all transmitted light (for a detailed description of the experimental setup, see Supporting Information, Figure 7). The hot carrier device produces a detectable and reliable current signal for $\lambda > 1.25$ μm, while the signal of the commercial detector fades dramatically as the wavelength of illumination increases beyond 1.1 μm. Note that this commercial Si detector generates very little current at $\lambda \sim 1.30$ μm (below Si bandgap energy, see Figure 5g), likely resulting from the presence of trap states within the semiconductor. These states subsequently increase the device dark current, which is detrimental to its performance. The commercial detector produces greater photoresponse near the bandgap (see Figure 5b,f for comparison), as expected because the hot carrier detector demonstrated in this paper is not optimized for wavelengths at or above the bandgap of Si. One strategy to further increase the performance of the Pt hot carrier device consists of heavily doping the Si layer at the metal−semiconductor interface to reduce the barrier height ($q\Phi_B$ in Figure 1b) and increase both the bandwidth and responsivity due to improved collection of photoexcited carriers from *d*-band states.[32] In this case, there is a trade-off because the increase in dark current must also be considered. Additionally, shrinking the overall device area can decrease the capacitance, which in turn, increases carrier collection efficiency.[33] Concerning alternative materials, metallic alloys could be used to tune the optical and electrical properties of the metal layer for greater light absorption and hot carrier collection in thin films.[14,34,35] Nevertheless, here we show a facile approach based on hot carrier generation that surpasses current commercial Si technology for room temperature, zero-bias, NIR detectors.

DOI: 10.1021/acsphotonics.7b01021
ACS Photonics 2018, 5, 306−311

CONCLUSION

In summary, we demonstrated hot carrier generation from NIR photon absorption (below the semiconductor bandgap) in ultrathin metal films, which represents an effective and low-cost solution to extend the bandwidth of semiconductor photodetectors and other optoelectronic devices. We have shown that by selecting materials with approximately equal real and imaginary parts of the refractive indices, such as Pt, Fe, Cr, and Ti, we can obtain nearly 80% absorption of broadband NIR light in a nanometer-scale planar metallic contact to Si. By contrast, traditional metals used for plasmonics and nanophotonics (e.g., Au, Ag, Cu, and Al) only allow for ∼20% optical absorption. We fabricated hot carrier near-IR photodetectors by depositing Pt on Si and obtained a 10^{-4} - 10^{-6} A/W photoresponse at zero applied bias for wavelengths of 1.2−1.5 μm, respectively, based on 16 nm of metal. Further, we have demonstrated its room temperature operation as an imaging detector with superior performance (operation below the semiconductor bandgap) compared to commercial Si detectors. The simplicity of the geometry and fabrication makes this hot carrier device concept straightforward for incorporation into current commercial fabrication methods. These concepts could also be expanded to metal−insulator−metal hot carrier systems to improve visible and ultraviolet performance.[36−38] Further, the development of a Si-based NIR detector for on-chip applications will likely have a significant impact on both Si photonics and telecommunications devices, where NIR detection is difficult to achieve using a single semiconductor platform.

METHODS

Sample Fabrication. All devices were fabricated on 368 μm thick, double side polished, <100> *n*-type silicon wafers (1−10 Ω·cm). Wafers were cleaned in a piranha etch (3:1 sulfuric acid (H_2SO_4) and hydrogen peroxide (H_2O_2)) to remove all organic material. A buffered oxide etch (BOE) was used to remove the native oxide, and dried under an N_2 stream. Immediately after the cleaning procedure, ohmic contacts were formed by depositing aluminum (Al) through a shadow mask in a thin strip along the top surface of each device, which was annealed at 425 °C in a forming gas of 96% Ar and 4% H_2. Then a ∼170 nm SiN_x antireflection coating was deposited using an Oxford plasma enhanced chemical vapor deposition (PECVD) system through a shadow mask, keeping the Al uncoated to enable electrical connection to the device. Finally, the native oxide was removed from the back surface of the Si with BOE, and the absorbing ultrathin metal contacts were deposited using an Angstrom e-beam evaporator at a deposition rate of ∼1 Å s^{-1} at a pressure of ∼2 × 10^{-6} Torr through a shadow mask, allowing for multiple metal thicknesses to be deposited on the same device.

Optical and Electrical Measurements. Specific wavelengths were selected from a supercontinuum source (Fianium WhiteLase) using an acousto-optic tunable filter (AOTF). Absorption measurements were performed using a 6 in. integrating sphere (Labsphere RTC-060) with illumination at near-normal incidence of 12°. One Ge photodiode was used to measure the light intensity inside the integrating sphere, and a second was used to monitor power fluctuations of the incident beam. The signal from each photodiode and the photocurrent from the hot carrier detectors were measured using a SR830 lock-in amplifier. The power incident on the sample was measured using a calibrated Ge photodiode to calculate the responsivity. To determine barrier height, *IV* curves were acquired (see see Supporting Information, Figure 5) using a Keithley 2400 source meter, with current and voltage recorded using a custom-built LabVIEW script.

Imaging Detector. The maps in Figure 5 were obtained using a confocal optical microscope in transmission mode. The microscope was modified to focus the beam of the supercontinuum laser source with a 60× bottom objective (NA = 0.7), illuminating the Au/Quartz sample. The detectors were mounted to collect light through a 20× objective (NA = 0.4).

ASSOCIATED CONTENT

Supporting Information

The Supporting Information is available free of charge on the ACS Publications website at DOI: 10.1021/acsphotonics.7b01021.

Description of analytical calculations for absorption in thin films and reflection from silicon nitride antireflection coating, effect of illumination direction on absorption and photoresponse, responsivity comparison for illumination on and off the absorbing Schottky contact, electrical device characterization and fit to thermionic emission model, comparison of hot carrier detector with commercial Si detectors, experimental setup for NIR imaging, and detectivity of hot carrier detector (PDF).

AUTHOR INFORMATION

Corresponding Author

*E-mail: jnmunday@umd.edu.

ORCID

Elizabeth M. Tennyson: 0000-0003-0071-8445
Marina S. Leite: 0000-0003-4888-8195
Jeremy N. Munday: 0000-0002-0881-9876

Author Contributions

L.J.K. performed the calculations, carried out sample fabrication, and performed optical and electrical measurements. L.J.K. and E.M.T. performed imaging experiments. L.J.K. and J.N.M. designed the experiments and analyzed the results. J.N.M. conceived and supervised the project. All authors contributed to the design of the optical setup for transmission images, discussed the results, and contributed to the manuscript preparation.

Notes

The authors declare no competing financial interest.

ACKNOWLEDGMENTS

This material is based upon work supported by the National Science Foundation CAREER Grant No. ECCS-1554503 and the Office of Naval Research YIP Award under Grant No. N00014-16-1-2540. The authors also acknowledge support from the FabLab at the Maryland NanoCenter. L.J.K. is supported by a NSF Graduate Research Fellowship, DGE 1322106. E.M.T. acknowledges a 2016-2017 UMD Dean's Dissertation Fellowship. The authors also thank J. Murray, T. Narayan, and K. Palm for providing the imaging object for the detectors.

REFERENCES

(1) Soref, R. Mid-Infrared Photonics in Silicon and Germanium. *Nat. Photonics* **2010**, *4*, 495−497.

DOI: 10.1021/acsphotonics.7b01021
ACS Photonics 2018, 5, 306−311

(2) Asghari, M.; Krishnamoorthy, A. V. Silicon Photonics: Energy-Efficient Communication. *Nat. Photonics* **2011**, *5*, 268−270.
(3) Reed, G. T.; Mashanovich, G.; Gardes, F. Y.; Thomson, D. J. Silicon Optical Modulators. *Nat. Photonics* **2010**, *4* (8), 518−526.
(4) Liang, D.; Bowers, J. E. Recent Progress in Lasers on Silicon. *Nat. Photonics* **2010**, *4* (8), 511−517.
(5) Michel, J.; Liu, J.; Kimerling, L. C. High-Performance Ge-on-Si Photodetectors. *Nat. Photonics* **2010**, *4*, 527−534.
(6) Kang, Y.; Liu, H.-D.; Morse, M.; Paniccia, M. J.; Zadka, M.; Litski, S.; Sarid, G.; Pauchard, A.; Kuo, Y.-H.; Chen, H.-W.; Zaoui, W. S.; Bowers, J. E.; Beling, A.; Mcintosh, D. C.; Zheng, X.; Campbell, J. C. Monolithic Germanium/silicon Avalanche Photodiodes with 340 GHz Gain− Bandwidth Product. *Nat. Photonics* **2009**, *3*, 59−63.
(7) Ye, N.; Gleeson, M. R.; Sadiq, M. U.; Roycroft, B.; Robert, C.; Yang, H.; Zhang, H.; Morrissey, P. E.; Mac Suibhne, N.; Thomas, K.; Gocalinska, A.; Pelucchi, E.; Phelan, R.; Kelly, B.; OCarroll, J.; Peters, F. H.; Garcia Gunning, F. C.; Corbett, B. InP-Based Active and Passive Components for Communication Systems at 2 Mm. *J. Lightwave Technol.* **2015**, *33* (5), 971−975.
(8) Wirths, S.; Geiger, R.; Von Den Driesch, N.; Mussler, G.; Stoica, T.; Mantl, S.; Ikonic, Z.; Luysberg, M.; Chiussi, S.; Hartmann, J. M.; Sigg, H.; Faist, J.; Buca, D.; Grützmacher, D. Lasing in Direct-Bandgap GeSn Alloy Grown on Si. *Nat. Photonics* **2015**, *9*, 88−92.
(9) Mączko, H. S.; Kudrawiec, R.; Gladysiewicz, M. Material Gain Engineering in GeSn/Ge Quantum Wells Integrated with an Si Platform. *Sci. Rep.* **2016**, *6* (1), 34082.
(10) Ackert, J. J.; Thomson, D. J.; Shen, L.; Peacock, A. C.; Jessop, P. E.; Reed, G. T.; Mashanovich, G. Z.; Knights, A. P. High-Speed Detection at Two Micrometres with Monolithic Silicon Photodiodes. *Nat. Photonics* **2015**, *9*, 393−397.
(11) Grote, R. R.; Padmaraju, K.; Souhan, B.; Driscoll, J. B.; Bergman, K.; Osgood, R. M., Jr. 10 Gb/s Error-Free Operation of All-Silicon Ion-Implanted-Waveguide Photodiodes at 1.55 Mm. *IEEE Photonics Technol. Lett.* **2013**, *25* (1), 67−70.
(12) Knight, M. W.; Sobhani, H.; Nordlander, P.; Halas, N. J. Photodetection with Active Optical Antennas. *Science (Washington, DC, U. S.)* **2011**, *332* (6030), 702−704.
(13) Li, W.; Valentine, J. Metamaterial Perfect Absorber Based Hot Electron Photodetection. *Nano Lett.* **2014**, *14* (6), 3510−3514.
(14) Scales, C.; Berini, P. Thin-Film Schottky Barrier Photodetector Models. *IEEE J. Quantum Electron.* **2010**, *46* (5), 633−643.
(15) Kosonocky, W. F. Review of Schottky-Barrier Imager Technology. *Proc. SPIE* **1990**, *1308*, 2−26.
(16) Chen, C. K.; Nechay, B.; Tsaur, B.-Y. Ultraviolet, Visible, and Infrared Response of PtSi Schottky-Barrier Detectors Operated in the Front-Illuminated Mode. *IEEE Trans. Electron Devices* **1991**, *38* (5), 1094−1103.
(17) Hägglund, C.; Apell, S. P.; Kasemo, B. Maximized Optical Absorption in Ultrathin Films and Its Application to Plasmon-Based Two-Dimensional Photovoltaics. *Nano Lett.* **2010**, *10*, 3135−3141.
(18) Llorens, J. M.; Buencuerpo, J.; Postigo, P. A. Absorption Features of the Zero Frequency Mode in an Ultra-Thin Slab. *Appl. Phys. Lett.* **2014**, *105* (23), 231115.
(19) Kats, M. A.; Blanchard, R.; Genevet, P.; Capasso, F. Nanometre Optical Coatings Based on Strong Interference Effects in Highly Absorbing Media. *Nat. Mater.* **2013**, *12*, 20−24.
(20) Mirshafieyan, S. S.; Guo, H.; Guo, J. Zeroth Order Fabry−Perot Resonance Enabled Strong Light Absorption in Ultrathin Silicon Films on Different Metals and Its Application for Color Filters. *IEEE Photonics J.* **2016**, *8* (5), 1−12.
(21) Song, H.; Guo, L.; Liu, Z.; Liu, K.; Zeng, X.; Ji, D.; Zhang, N.; Hu, H.; Jiang, S.; Gan, Q. Nanocavity Enhancement for Ultra-Thin Film Optical Absorber. *Adv. Mater.* **2014**, *26* (17), 2737−2743.
(22) Dotan, H.; Kfir, O.; Sharlin, E.; Blank, O.; Gross, M.; Dumchin, I.; Ankonina, G.; Rothschild, A. Resonant Light Trapping in Ultrathin Films for Water Splitting. *Nat. Mater.* **2012**, *12* (2), 158−164.
(23) Driessen, E. F. C.; de Dood, M. J. A. The Perfect Absorber. *Appl. Phys. Lett.* **2009**, *94* (17), 171109.
(24) Park, J.; Kang, J.-H.; Vasudev, A. P.; Schoen, D. T.; Kim, H.; Hasman, E.; Brongersma, M. L. Omnidirectional Near-Unity Absorption in an Ultrathin Planar Semiconductor Layer on a Metal Substrate. *ACS Photonics* **2014**, *1*, 812−821.
(25) Palik, E. D. *Handbook of Optical Constants of Solids, I-III*; Elsevier Inc: Amsterdam, 1998.
(26) Weaver, J. H.; Colavita, E.; Lynch, D. W.; Rosei, R. Low-Energy Interband Absorption in Bcc Fe and Hcp Co. *Phys. Rev. B: Condens. Matter Mater. Phys.* **1979**, *19* (8), 3850−3856.
(27) Zhukov, V. P.; Chulkov, E. V.; Echenique, P. M. Lifetimes and Inelastic Mean Free Path of Low-Energy Excited Electrons in Fe, Ni, Pt, and Au: Ab Initio GW+ T Calculations. *Phys. Rev. B: Condens. Matter Mater. Phys.* **2006**, *73*, 125105.
(28) Dey, P.; Weber, W.; Inomata, K.; Ikeda, N.; Tezuka, N.; Offi, F.; Iacobucci, S.; Petaccia, L.; Johnson, P. D.; Altman, M. S.; Yasuda, M.; Tamura, K.; Kawata, H.; Zdyb, R.; Bauer, E. Spin-Resolved Inelastic Mean Free Path of Slow Electrons in Fe. *J. Phys.: Condens. Matter* **2013**, *25* (25), 272201−272204.
(29) Ding, Z.-J.; Shimizu, R. A Monte Carlo Modeling of Electron Interaction with Solids Including Cascade Secondary Electron Production. *Scanning* **1996**, *18* (2), 92−113.
(30) Dalal, V. L. Simple Model for Internal Photoemission. *J. Appl. Phys.* **1971**, *42* (6), 2274−2279.
(31) Mönch, W. On Metal-Semiconductor Surface Barriers. *Surf. Sci.* **1970**, *21* (2), 443−446.
(32) Zheng, B. Y.; Zhao, H.; Manjavacas, A.; McClain, M.; Nordlander, P.; Halas, N. J. Distinguishing between Plasmon-Induced and Photoexcited Carriers in a Device Geometry. *Nat. Commun.* **2015**, *6*, 7797.
(33) Casalino, M.; Coppola, G.; Gioffre, M.; Iodice, M.; Moretti, L.; Rendina, I.; Sirleto, L. Cavity Enhanced Internal Photoemission Effect in Silicon Photodiode for Sub-Bandgap Detection. *J. Lightwave Technol.* **2010**, *28* (22), 3266−3272.
(34) Gong, C.; Leite, M. S. Noble Metal Alloys for Plasmonics. *ACS Photonics* **2016**, *3* (4), 507−513.
(35) Gong, T.; Munday, J. N. Materials for Hot Carrier Plasmonics [Invited]. *Opt. Mater. Express* **2015**, *5* (11), 2501.
(36) Wang, F.; Melosh, N. A. Plasmonic Energy Collection through Hot Carrier Extraction. *Nano Lett.* **2011**, *11*, 5426−5430.
(37) Gong, T.; Munday, J. N. Angle-Independent Hot Carrier Generation and Collection Using Transparent Conducting Oxides. *Nano Lett.* **2015**, *15*, 147−152.
(38) Gong, T.; Munday, J. N. Aluminum-Based Hot Carrier Plasmonics. *Appl. Phys. Lett.* **2017**, *110*, 21117.

DOI: 10.1021/acsphotonics.7b01021
ACS Photonics 2018, 5, 306−311